Sensors & Actuators: B. Chemical 444 (2025) 138504

Contents lists available at ScienceDirect

Sensors and Actuators: B. Chemical

journal homepage: www.elsevier.com/locate/snb

Photosensitivity and gas sensing mechanisms: Validation of an *operando* DRIFT spectroscopy apparatus for light-activated chemoresistive gas sensors

Emanuela Tavaglione [a], Elena Spagnoli [a], Matteo Valt [b], Paolo Bernardoni [c], Michele Della Ciana [a], Federico Bottegoni [d], Margherita Negri [d], Francesco Scali [d], Carlo Zucchetti [d], Matteo Ferroni [e], Matteo Ardit [f], Lia Vanzetti [b], Vito Cristino [g], Francesco Di Benedetto [a], Barbara Fabbri [a,*]

[a] Department of Physics and Earth Sciences, University of Ferrara, Via Saragat 1/C, Ferrara 44122, Italy
[b] Sensors and Devices center, Bruno Kessler Foundation, Via Sommarive 18, Trento 38123, Italy
[c] Department of Chemical, Pharmaceutical and Agricultural Sciences, University of Ferrara, via Luigi Borsari 46, Ferrara 44121, Italy
[d] Department of Physics, Politecnico di Milano, Piazza Leonardo da Vinci 32, Milano 20133, Italy
[e] Institute for Microelectronics and Microsystems IMM-CNR, Via Gobetti 101, Bologna 40129, Italy
[f] Department of Geosciences, University of Padova, Via Gradenigo 6, Padova 35131, Italy
[g] Department of Environmental and Prevention Sciences, University of Ferrara, Palazzo Turchi di Bagno, C.so Ercole I D'Este, 32, Ferrara 44121, Italy

ARTICLE INFO

Keywords:
Operando approach
DRIFT spectroscopy
Photoactivation
Gas sensing mechanism
Zinc oxide
Photocurrent

ABSTRACT

Despite the large number of published articles, several key questions concerning the light activation of the gas sensitivity in semiconductors are still open. The primary goal of this work is to validate a novel add-on tool for investigating gas–solid interactions at the chemoresistive sensor surface under operating conditions, using *operando* diffuse reflectance infrared Fourier transform spectroscopy. The innovative apparatus was designed to support a robust analysis of the sensing material properties for photoactivated applications, filling up the current knowledge gap concerning the involved physical and chemical reaction processes. Moreover, the design of a customized sample holder enables *in-situ* diffuse reflectance Fourier infrared spectroscopy measurements on irradiated functional powders, thereby limiting the signal-to-noise ratio and collecting additional information on chemisorption processes. The validation was conducted on a gold standard material for the photoactivation procedure, namely zinc oxide. The ZnO-based gas sensor was photoactivated at three different wavelengths (385, 468, and 525 nm) and the ZnO functional powder at 385 nm, by using commercial LEDs. The measurements were performed with an oxidizing and a reducing gas, *i.e.* NO_2 and ethanol, along with humidity. The distinctive peaks observed in *operando* and *in-situ* absorbance spectra revealed the presence of the target gases at the sensing layer, responsible for the corresponding changes in the sensor signal. These results confirmed the feasibility of employing the proposed setup to investigate photoactivated gas–solid interactions, while the method and setup account for geometry and illumination, ensuring reliable and comparable measurements.

1. Introduction

Chemoresistive gas sensors based on metal-oxide semiconductors (SMOXs) operating at room (RT) or low temperature represent a flourishing field of advanced electronic devices, encompassing the challenges associated with the usually required high operating temperatures (200 – 500 °C), namely high power consumption, reduced sensor lifetime, and unsuitability for harsh and delicate environments [1,2]. Nevertheless, non-thermoactivated gas sensors commonly result in low sensitivity and slow response and recovery time [3,4], because adsorption processes on their surface require a non-negligible activation energy, ranging from 10 meV to 1 eV [5]. Hence, light activation has emerged as a potential alternative to thermal activation. Indeed, a proper illumination can change the sensing material's reactivity by increasing the surface carrier

* Corresponding author.
E-mail address: barbara.fabbri@unife.it (B. Fabbri).

https://doi.org/10.1016/j.snb.2025.138504
Received 6 February 2025; Received in revised form 7 August 2025; Accepted 8 August 2025
Available online 9 August 2025

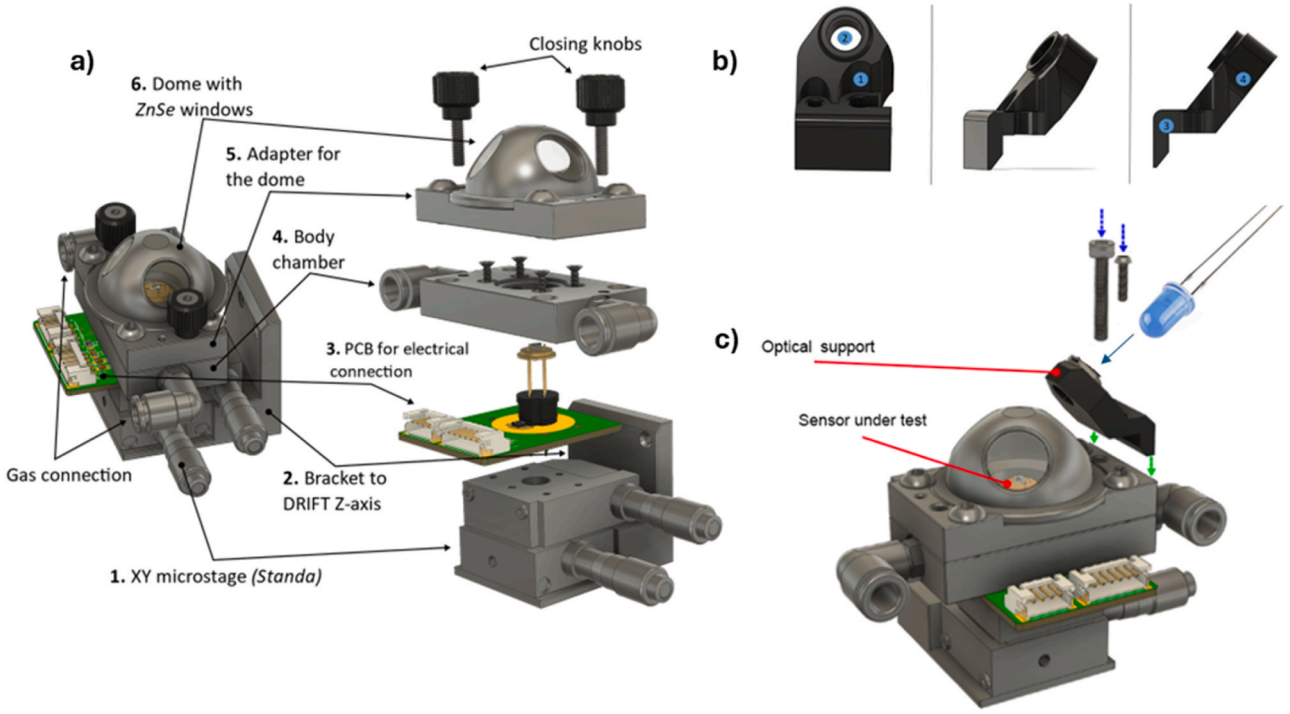

Fig. 1. a) Reaction chamber design and electronics description. b) ① screw hole to fix the add-on tool to the main body cell; ② hole designed for the LED positioning; b) ③ and ④ lower part and upper part of the add-on tool, respectively. c) Reaction chamber with add-on tool, namely LED support.

density [1]. In the case of a direct band gap semiconductor, the excitation of electrons from the valence band (*VB*) to the conduction band (*CB*) can be accomplished via light with a photon energy matching the band gap E_g of the material. Most SMOXs are wide band-gap semiconductors and, in principle, at least Ultraviolet (UV) light is needed to generate photocarriers. Moreover, the semiconductor's defectivity results in the formation of deep donor levels within the band gap, thereby significantly impacting optical processes. Indeed, it is possible to introduce defectivities into the material, *e.g.,* by doping, to enhance the photosensitivity of the sensing layer, as these promote the formation of impurity absorption states at lower energy with respect to E_g [6]. Understanding the reactions that occur at the surface in photo-activation mode is an important task, as these reactions may differ from those observed in thermoactivated sensors, involving physico-chemical phenomena that have not been completely explored so far [7]. Although some literature reports have partially addressed this topic from a theoretical point of view [8,9], experimental evidence of the phenomena leading to photoactivation are still missing [1,8,10,11]. Therefore, a systematic experimental investigation of this field is mandatory, and it can be properly performed by means of an *operando* approach, to monitor the reactions between the sensing layer and the analytes during the sensor operation. Advancements have been made in the *operando* direction [12], yet further research is necessary to ensure the reproducibility and comparability of measurements while maintaining experimental flexibility. The development of a more analytical method and a configuration that takes into account geometry and illumination factors is imperative.

The Sensors Laboratory at the University of Ferrara (UNIFE) has already employed the *operando* Diffuse Reflectance Infrared Fourier Transform (DRIFT) spectroscopy to investigate the chemical species interacting with the sensing layer of thermoactivated devices while obtaining electrical measurements [13–15]. The aim of this work was to extend the functionality of the apparatus for *operando* DRIFT experiments in photo-activation mode. The instrumental setup was achieved through the implementation of an innovative add-on tool, which ensures fixed positioning of the light source (*e.g.,* LED) relative to the sensor, avoiding distance fluctuations. Additionally, the setup facilitates an easy replacement of LEDs to explore different wavelengths, offering flexibility for diverse experimental requirements and aiming to go beyond the extensive research focused on UV-light activated MOX gas sensors.

A zinc oxide-based gas sensor was selected for validation due to its status as a leading material in the field of chemoresistive gas sensing applications both in thermo- and photoactivation, making it a gold standard. ZnO is a direct wide band-gap semiconductor ($E_g \sim 3.37$ eV), hence a large number of photocarriers are generated when illuminated with a radiation wavelength corresponding to UV light [8]. In this work, the photoresponse of the ZnO-based sensor was evaluated under three distinct wavelengths, 385 nm (UV), 468 nm (blue), 525 nm (green), properly calibrated. The *operando* apparatus, which simultaneously conducts electrical measurements and DRIFT spectroscopy, was subsequently used to investigate surface reactions on the ZnO surface under UV, blue, or green LED photoactivation, in the presence of both oxidizing and reducing gases, specifically nitrogen dioxide and ethanol, and humidity.

The small sensitive area of the device and the low intensity of the infrared (IR) signal in the diffuse reflectance configuration, could impede the detection of subtle changes in surface chemical species, such as a negligible shift in surface chemistry resulting from low probability reactions. However, these may still contribute to the sensor signal, which is generally lower in photo- than in thermo-activation mode, as a clear indication that the surface redox reactions are less consistent in number. Hence, a sample holder was employed to host the nanostructured ZnO powder, thereby expanding the area under examination and enabling the employment of a larger IR spot. A deeper understanding of the SMOX/gas interaction in photoactivation was gained by analyzing the DRIFT spectra. The nanostructured powder was illuminated with the radiation wavelength at which the ZnO-based sensor exhibited optimal performance. The powder was then exposed to NO_2, ethanol and relative humidity (RH%), as performed on the ZnO-based sensor.

Ultimately, this work aimed to further explore the understanding of the photosensitivity of functional materials and the sensing processes

occurring at the gas-solid interface during photoactivation. This research has the potential to contribute to significant advancements in the development of RT gas sensor technologies.

2. Materials and methods

2.1. Nanopowder characterization and sensor preparation

ZnO was prepared through a precipitation method involving zinc acetate dihydrate as precursor. An annealing treatment at 650 °C was applied to obtain a nanosized crystalline powder. The material was morphologically, chemically and structurally characterized by Scanning Electron Microscopy (SEM), Energy Dispersion X-Ray spectroscopy (EDX), X-ray Powder Diffraction (XRPD), X-ray Photoelectron Spectroscopy (XPS). Ultraviolet-visible spectroscopy (UV–vis) analysis was carried out to determine the material's optical properties, whereas electron paramagnetic resonance (EPR) measurements were performed to investigate its defectivity.

The functional material was then used to prepare a screen-printed thick-film (1 mm^2 x 20 μm) sensor (Fig. S1 and S2).

All specifications about nanopowder synthesis, sensor preparation, instruments, equipment, data collection and evaluation are reported in the Supporting Information.

2.2. Sensing film characterization

2.2.1. Photocurrent measurements

Photocurrent measurements were performed at RT on the ZnO sensor mounted on a TO39 support (Fig. S3) [16–18]. All specifications are available in the Supporting Information.

2.2.2. Operando DRIFT measurements

2.2.2.1. Experimental setup. The setup is based on a Bruker Vertex 70 v Fourier-transform infrared spectroscopy (FTIR) spectrometer equipped with the Praying Mantis optical accessory by Harrick Scientific to enable DRIFT measurements (Fig. S4). The 3D drawing in Fig. 1a represents the customized reaction test chamber, located inside the mirror optics and housing the gas sensor [14,19]. All specifications of the apparatus provided by the manufacturer, as well as previously published system upgrades, are described in the Supporting Information.

The *operando* DRIFT spectroscopy system was then extended with a custom add-on tool, properly designed on Fusion360 and 3D printed in matte black PLA, shown in Fig. 1b, that allowed analysis of surface reactions in photo-activation mode. Another hole for the screw (Fig. 1b ①) was required to isolate the internal dome environment and to attach the add-on tool to the main body cell. The LED positioning hole (Fig. 1b ②) was designed to allow stable placement of the commercial bulb LED, as close as possible to the dome front SiO_2 window. The main body of the tool (Fig. 1b ③ and ④) was designed to be tilted as the window (Fig. 1c) to achieve the maximum irradiation of the sensing layer. The vacuum flange was also modified to allow the presence of the LED in the chamber and the connection to a Keithley - K2000 as power source (Fig. S5a). A picture of the set-up with a blue LED on is shown in Fig. S5b.

This work emphasizes the importance of providing details on the sensor's applied voltage and the light irradiance on the sensing layer to allow comparability between data. The bias voltage promotes the separation of photogenerated charge carriers, alters carrier drift velocity, and influences their lifetime and density, all of which have a substantial impact on sensor performance [9]. Moreover, it is crucial to determine the light irradiance received by the sensing layer, as it has an impact on the material's photoresponse. Other information, such as light source parameters or its distance from the sensing layer, is of secondary importance because the photon flux may encounter light interferences and barriers, *e.g.,* quartz glass, along its path. Irradiance is the power per unit area received by a surface when exposed to electromagnetic radiation. It quantifies the amount of radiant energy (such as light) that falls onto a unit area of a surface per unit time. Irradiance depends on the intensity and distance of the light source, which in this case is fixed. Each light source used, UV (385 nm), blue (468 nm), and green (525 nm), see Table S1 in the Supporting information, was calibrated with a Hamamatsu Si photodiode S1336 series having the same geometry as the gas sensors produced at UNIFE (TO-39 package). The irradiance on the surface of the sensor was 9 $\frac{mW}{cm^2}$ and considering the sensing area (1 mm^2), the study on spatial distribution on illumination (Fig. S6-S8) revealed an irradiance uniformity. More information about LEDs calibration is provided in the Supporting Information. Furthermore, these light sources can be used safely to irradiate the sensor without interfering with the MCT detector of the FTIR spectrometer, which can detect wavelengths from 833 nm to 12 μm. In this study, the irradiation and the applied voltage were held constant for validation purposes, however, the system may be used in future research to examine the material's performance under various voltage and irradiance settings.

In order to take advantage of the physico-chemical adsorption processes occurring at ZnO-gas interface, the experimentation provided further DRIFT measurements on the pure ZnO powder properly housed in a custom-made crucible that addressed the test chamber geometry (Fig. S9). This configuration enabled the use of a larger IR spot of 3.5 mm, instead of 2.5 mm used for the sensing film, thus increasing the area involved in the analysis. A detailed description of such add-ons can be found in the Supporting information.

2.2.2.2. Electrical measurements. The *operando* DRIFT setup was validated through three main steps: (i) assessment of the ZnO-based sensor photoresponse at RT in synthetic air (20 % O_2, 80 % N_2) under dark condition and under selected LED irradiation; (ii) electrical characterization in presence of NO_2 and ethanol gases from certified cylinders; (iii) evaluation of humidity effects.

For both (ii) and (iii), the sensor signal baselines were stabilized at the beginning of each measurement by keeping the sensors illuminated with the LED and in a steady flow (100 sccm) of dry air. Then, 2 ppm of NO_2, 50 ppm of ethanol or a fixed water vapor concentration (20 RH%) was fluxed into the test chamber for 30 min to collect the sensor response. Synthetic dry air was introduced at the end of each measurement to recover the baseline. The target gas concentrations were chosen considering the analytes threshold limit value (TLV), namely 2 ppm for NO_2 and 1000 ppm for ethanol. The humidity level of 20 RH% was chosen because it is a concentration above which the performances of MOX-based gas sensors result stable [10].

Resistance measurements of the sensing film over the time were obtained applying a constant bias voltage of 2 V to the film.

The ZnO-based sensor is an n-type semiconductor. Hence, its responses were calculated as:

$$\frac{(R_{baseline} - R_{gas})}{R_{gas}} \text{ for reducing gases} \quad (1)$$

$$\frac{(R_{gas} - R_{baseline})}{R_{baseline}} \text{ for oxidizing gases} \quad (2)$$

where $R_{baseline}$ and R_{gas} are the sensor resistance at the baseline (dry air) and after gas injection, respectively.

The response and recovery times were estimated as the time needed to attain 90 % of the response value and the time required to return to 90 % of the baseline value, respectively.

2.2.2.3. DRIFT spectra acquisition. *Operando* DRIFT spectra were collected with a resolution of 1 cm^{-1} and as an average of 1024 scans. The IR spectra were processed by Bruker's OPUS software. To determine material surface variations due to changes in ambient gas composition,

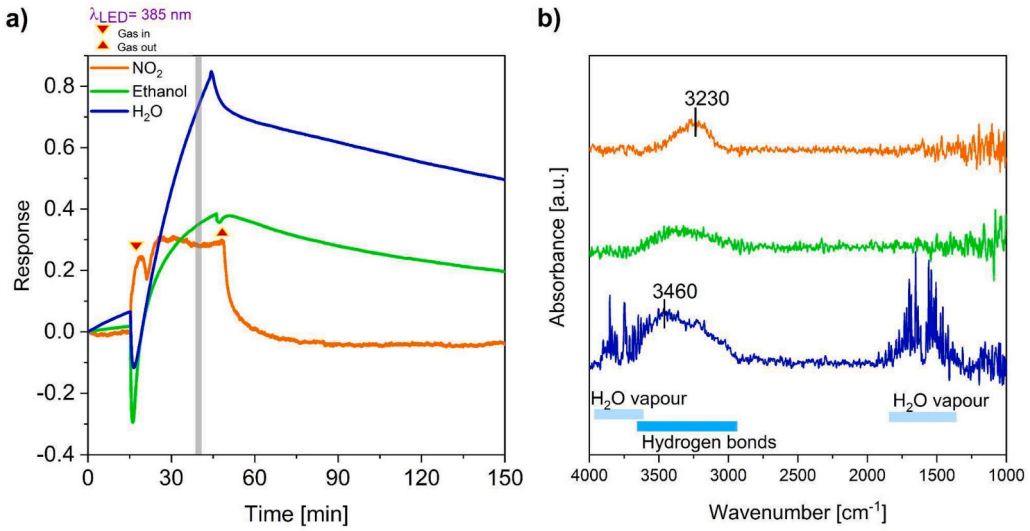

Fig. 2. a) Resistance and b) *AB* spectra of a pure ZnO-based sensor irradiated with 385 nm, in dry condition, exposed to 2 ppm of NO_2 (orange line), 50 ppm of ethanol (green line) and 20 % of RH (blue line), respectively. The gray vertical bar in a) represents the *AB* spectra scan in b).

absorbance spectra were calculated as apparent absorbance (*AB*) using:

$$AB(\lambda) = -log_{10}(I_{sample}(\lambda)/I_{background}(\lambda)) \quad (3)$$

where $I_{sample}(\lambda)$ and $I_{background}(\lambda)$ are the intensity of the spectrum of the sample recorded during exposure to synthetic air and recorded during exposure to the target gas, respectively.

AB spectra were acquired directly over the surface of the sensing film at specific time intervals during the electrical measurements. Acquisitions were made during i) baseline, ii) steady state (around 25 min after gas injection), and iii) recovery (90 min after returning to air) [13,20].

Regarding the pure functional material, *AB* spectra were collected over the top surface of the powder in the crucible. Data were acquired i) during dry air stabilization, ii) 30 min after the gas injection, and iii) 30 min after return to baseline.

The three scans were collected to observe the formation of distinctive peaks in the spectra and their eventual disappearance after recovery.

3. Results

3.1. Material morphological, chemical, and structural characterization

3.1.1. SEM-EDX analysis

The morphologies of the synthesized materials were investigated through SEM analysis. The pure ZnO grains in Fig. S10a and S10b (at two different magnifications) showed an irregular spherical shape. Adjacent particles appeared to share their boundaries as in an intermediate state of coarsening, possibly as a consequence of the relatively high calcination temperature (650 °C). The material was homogeneous, in fact each grain had a diameter of approximately 100 nm. EDX analyses allowed the observation and characterization of the basic components present in the materials (see Fig. S10c). The main components of the powder were Zn and O, with impurities of C, due to the carbon-based composition of the adhesive surface on which the sample was deposited.

3.1.2. XRD analysis

The diffraction pattern of ZnO grains in Fig. S11 shows that the powders were monophasic, composed of zincite with space group $P6_3mc$, *i.e.,* wurtzite-type structure and hexagonal phase. The unit cell parameters and cell volume, with their standard deviations, are summarized in Table S2 together with the crystallite size.

3.1.3. XPS analysis

The surface composition of ZnO was investigated by XPS analysis. Fig. S12 shows the survey XPS spectra acquired in the range of binding energies 5 − 1200 eV, highlighting the presence of Zn, O and C. The atomic percentage (at%), resulting from core lines and atomic sensitivity factors, are listed in Table S3. Pure ZnO exhibited an at% ratio of Zn and O corresponding to the stoichiometry (1:1) of the metal oxide.

3.1.4. UV–vis analysis

UV–visible analysis was conducted on pure ZnO to obtain the Tauc plot shown in Fig. S13. The direct optical band gap extrapolated through the straight-line portion of the Tauc plots is $E_g \sim 3.24$ eV.

3.1.5. EPR analysis

EPR measurements on ZnO nanopowder [21] highlighted the presence of a signal at g-factor = 1.96 (Fig. S14), distinctive of the formation of trapped electron centers [22,23].

3.2. Film photocurrent characterization

A clear photocurrent contribution was detected across the whole investigated photon energy range (Fig. S15a), including photon energies lower than the ZnO gap. As illustrated in Fig. S15b, the typical current-voltage dependence under illumination reveals a minimum photocurrent was detected at $V = -0.35$ V due to the lateral photovoltage, probably due to light absorption inhomogeneities or different Au/ZnO contact resistances between electrodes. For $V = -2$ V, the responsivity was found to be approximately one order of magnitude larger than the values in Fig. S15a, since the employed photon energy approaches the ZnO energy gap E_g. More detailed results are included in the Supporting Information.

3.3. System validation

3.3.1. Sensing film resistance in dark and light conditions

The resistance of the ZnO-based sensor at RT in dark and dry conditions (1 RH% and 28°C) was in the order of GΩ. However, precise measurement of this high resistance value was not feasible due to limitations of the available electronics. Upon exposure to UV light, a significant reduction in resistance (3.9 MΩ) was observed (Fig. S16). When the UV LED was deactivated, the resistance of the film gradually increased, suggesting a gradual recovery of the baseline in dark conditions. However, this effect did not influence the resistance observed

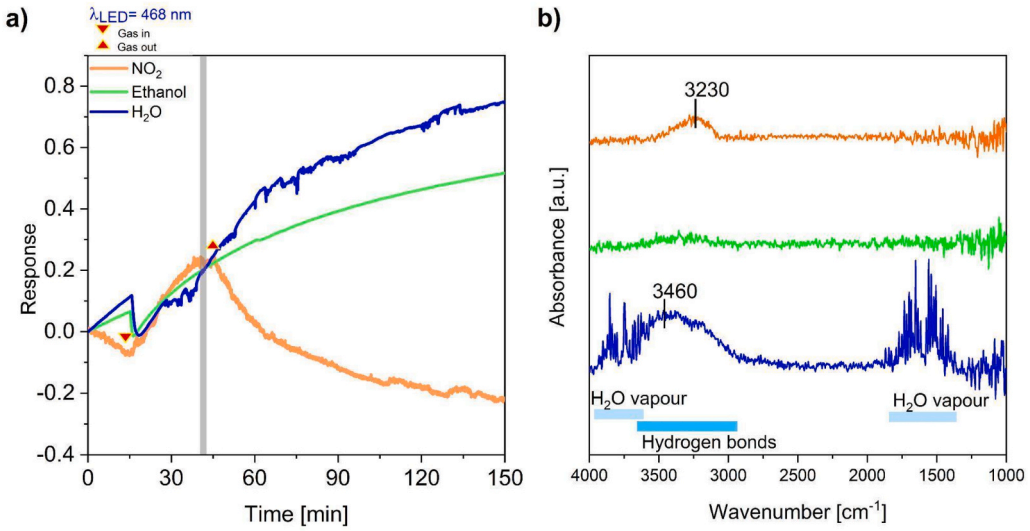

Fig. 3. a) Resistance and b) *AB* spectra of a pure ZnO-based sensor irradiated with 468 nm, in dry condition, exposed to 2 ppm of NO_2 (orange line), 50 ppm of ethanol (green line) and 20 % of RH (blue line), respectively. The gray vertical bar in a) represents the *AB* spectra scan in b).

under subsequent UV-light exposure (Fig. S16). The slow signal recovery subsequent to the interruption of irradiation can be ascribed to the persistent photoconductivity of the material, as documented in previous studies [24,25]. The single channel spectra acquired in dark and under UV irradiation over the ZnO sensor in dry condition are shown in Fig. S17. Both spectra display the same peaks, indicating that the material in dry air interacts in the same way under both dark and UV-light conditions. As expected, the film resistance was higher under blue- and green-light irradiation than under UV light, namely 9.6 MΩ and 11.6 MΩ, respectively.

3.3.2. *Operando DRIFT measurements on ZnO sensor*

The ethanol and humidity sensor responses were calculated using Eq. (1), while the NO_2 response was calculated using Eq. (2). Negative values are plotted on the y-axis to highlight the sensor's dynamic signal, including possible baseline drift or unpredictable sensor behavior, such as an initial spike following each gas injection, due to a pneumatic effect (Fig. S18). To improve the clarity of the graphs, only the *AB* spectra acquired at steady state are shown. The Supporting information (Fig. S19) provides an example of the three scans performed under UV-light irradiation in the presence of 2 ppm of NO_2.

Fig. 2 summarizes electrical measurements and DRIFT spectra obtained during exposure to NO_2, ethanol and humidity under UV irradiation (385 nm) in dry air. The sensor response to 2 ppm of NO_2 promptly reached a steady state (orange curve in Fig. 2a). When the initial dry air conditions were restored, the baseline was fully recovered. In this case, the response and recovery time were calculated to be 9 min and 7 min, respectively. However, when exposed to 50 ppm of ethanol (green curve) and 20 RH% (blue curve) under the same light irradiation, the sensor signals increased but did not stabilize during the exposure time or return to the baseline after the initial conditions were restored.

The *AB* DRIFT spectra under UV irradiation (Fig. 2b) display a broad band in the 3600 −2900 cm^{-1} range for all the three analytes tested. The band exhibits a maximum in absorbance at 3230 cm^{-1} for NO_2, whereas for H_2O and ethanol the maximum in absorbance is observed at 3460 cm^{-1}.

When exposed to blue-light irradiation (468 nm) in presence of 2 ppm of NO_2 (Fig. 3a), the sensor response (orange curve) stabilized only at the end of the analyte injection period and then slowly returned to the initial value during the restoration of the fully dry condition,

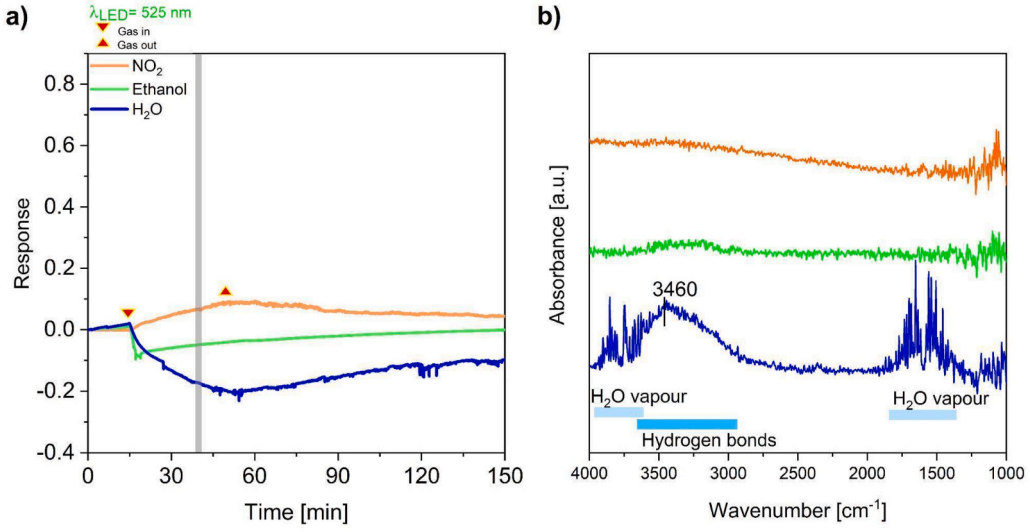

Fig. 4. a) Resistance and b) *AB* spectra of a pure ZnO-based sensor irradiated with 525 nm, in dry condition, exposed to 2 ppm of NO_2 (orange line), 50 ppm of ethanol (green line) and 20 % of RH (blue line), respectively. The gray vertical bar in a) represents the *AB* spectra scan in b).

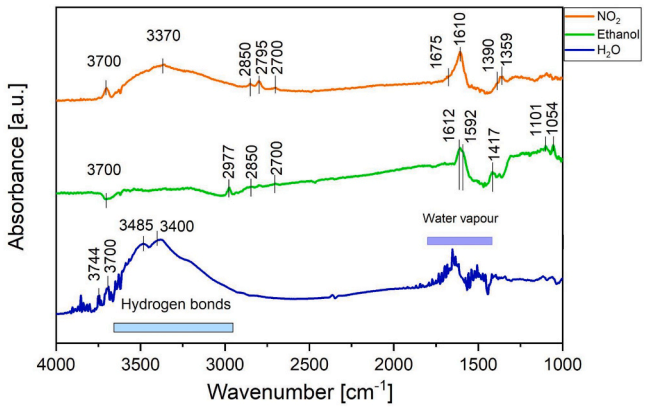

Fig. 5. *AB* spectra of pure ZnO nanostructured powder irradiated with 385 nm, in dry condition and exposed to 2 ppm of NO_2 (orange line), 50 ppm of ethanol (green line), and 20 % of RH (blue line).

maintaining the signal drift that also affected the baseline. Exposure to 50 ppm of ethanol (green curve) and 20 RH% (blue curve) did not significantly alter the film's resistance, which was primarily affected by the signal drift. The lack of sensor response may be due to the limited interaction between the gas and the surface under blue-light illumination.

The *AB* spectra obtained in presence of NO_2 and humidity (orange and blue curves, respectively) under blue-light irradiation (Fig. 3b) are similar to those obtained under UV light, showing a broad band in the 3600 −2900 cm^{-1} range that was not formed in the presence of ethanol (green curve).

Under green-light illumination (525 nm) and during the exposure to 2 ppm of NO_2 (Fig. 4a), the sensor's signal increased continuously and did not reach a plateau. Also in this case, the electrical resistance was not affected by 50 ppm of ethanol (green curve) and 20 RH% (blue curve), making it difficult to distinguish the sensor's response from the signal drift. The *AB* spectra acquired under green-light irradiation (Fig. 4b) showed no peaks in presence of NO_2 and ethanol.

In humid conditions, the AB spectra acquired under illumination with all three irradiation wavelengths revealed additional peaks in the ranges 1850 −1350 cm^{-1} and 4000 −3700 cm^{-1} attributable to the deformation vibration of physisorbed water molecules and to isolated −OH groups, respectively, as shown in Figs. 2b, 3b, and 4b [15].

3.3.3. *In-situ DRIFT measurements on the powder under UV radiation*

Fig. 5 shows the spectra obtained on the ZnO powder during exposure to 2 ppm of NO_2 (orange line), 50 ppm of ethanol (green line) and 20 % of RH (blue line).

The *AB* spectrum in presence of NO_2 (orange line in Fig. 5) displays a peak at 3700 cm^{-1}, typical of isolated −OH groups, and a broad band centered in the range 3600 −2900 cm^{-1}, indicating the formation of hydrogen bonds attributed to the physisorption of both NO_2 and H_2O. Peaks at 2850 cm^{-1}, 2795 cm^{-1} and 2700 cm^{-1} represent combination and overtone vibration of nitrato species [26]. The large peak at 1610 cm^{-1}, which represents monolayers of molecularly adsorbed water (O−H stretching mode) [27], is partially covering the peak at 1675 cm^{-1}, characteristic of adsorbed NO_2 [28,29]. Peaks at 1390 cm^{-1} and 1359 cm^{-1} correspond to bidentate nitrate [28,30].

The *AB* spectrum acquired during exposure to ethanol (green line) displays peaks at 2977 cm^{-1}, 2850 cm^{-1} and 2700 cm^{-1}, typical of ethoxy species. These latter may consume −OH groups, resulting in a downward peak at 3700 cm^{-1}. Nevertheless, the peak at 1612 cm^{-1} reveals that molecular water is still adsorbed on the surface. Moreover, the peak at 1592 cm^{-1} indicates the formation of acetate species [31], while the peak at 1417 cm^{-1} represents CH_3 and CH_2 scissoring mode [32]. Finally, 1101 and 1054 cm^{-1} can be attributed to monodentate and bidentate carbonates, respectively [33].

Water molecules are largely physisorbed on the ZnO powder surface when relative humidity is increased (blue line), as indicated by the strong intensity of the broad band in the range 3600 −2900 cm^{-1} of interacting −OH groups and the peak at 1610 cm^{-1} [27]. Additionally, part of the H_2O undergoes chemisorption, resulting in the formation of isolated −OH groups, as indicated by the peak at 3744 and 3700 cm^{-1} [34]. When a high water vapor content is reached in the test chamber, gaseous H_2O molecules contribute to absorption over wide regions of the mid-infrared spectrum (4000–3300 cm^{-1} and 2100–1300 cm^{-1}), resulting in sharp peaks [15].

4. Discussion

It is important to highlight that the preliminary LEDs calibration allowed for the experiment to be performed with the same irradiance conditions on the sensing layer. This ensured a uniform comparison of the electrical properties of the sensor at different wavelengths. Moving from dark to light condition, ZnO-based film exhibited the most significant resistance variation under UV-light irradiation, due to direct electron excitation from the *VB* to the *CB*. In contrast, under longer wavelength radiations, *i.e.* blue and green light, the electron excitation could only arise from intra-gap localized levels due to material defects. As expected, the film resistance was higher under 468 and 525 nm irradiation than under 385 nm. According to the UV–vis analysis, the band gap energy of the nanostructured ZnO powder was determined to be $E_g \sim 3.24$ eV (Fig. S13), a value that corresponds to a light with a wavelength of ~ 383 nm.

Nevertheless, the sensor's resistance in photo-activation mode by visible light was comparable to its response under UV-light irradiation (11.6 MΩ for green light, 9.6 MΩ for blue, and 3.9 MΩ for UV). The significant drop in resistance to visible light was likely due to the material's high defectivity. This high defectivity was exacerbated by two main effects. Firstly, the ZnO-based sensor exhibited a persistent photoconductivity switching from light to dark conditions (Fig. S16), *i.e.,* the sensor resistance did not immediately recover the value exhibited during the initial measure in dark condition. The origin of this phenomenon is usually attributed to the presence of oxygen vacancies (V_O) in the material [4,24]. In fact, when properly irradiated, V_O are ionized and release electrons [24]. Moreover, the irradiated V_O transition from a nonconducting ground state to a metastable conductive state [35]. In order to revert to the ground state, the metastable V_O must overcome a thermally activated barrier to recapture electrons. At RT, this process results in a long carrier lifetime [4]. Secondly, photocurrent analysis (Fig. S15) showed a contribution over the entire investigated photon energy range, including photon energies below E_g. This finding suggests the presence of multiple impurity absorption states within the E_g [35]. Indeed, the measured photocurrent intensity corresponding to photon energies in the near-infrared range could indicate photoexcitation from impurity states close to the ZnO *CB*, whereas the strong increase in responsivity by increasing the incident photon energy is indicative of the presence of other impurity states closer to the *VB* [36–38]. This is consistent with EPR analyses conducted on ZnO powders, which reveal a signal at g = 1.96, indicative of trapped electron centers. In particular, this states the presence of asymmetrical defects that might be trapped into oxygen vacancies. Indeed, the signal might be attributed to the creation of donor levels below the conduction band. This clarifies the role of visible light in promoting charge separation in polycrystalline ZnO.

It is well-known that under photoactivation, NO_2 induces oxidation of ZnO increasing the film resistance, whereas ethanol and H_2O promote its reduction leading to a decrease in resistance [9,39,40].

The optimal response and recovery kinetics were observed for NO_2 under UV light, considerably improved compared to those reported in previous studies [41], suggesting that the incident radiation is adequate to assist both adsorption and desorption, allowing the system to reach

equilibrium. In contrast, the lack of the stabilization of the signal and its recovery after the injection of H_2O and ethanol may be due to the absence of a dynamic equilibrium between adsorption and desorption processes, or from the progressive penetration of gas molecules into the porous sensing layer without effective photodesorption [8]. Indeed, under irradiation the energy provided by the incident photons may be insufficient to promote the desorption of strongly bound species.

The observed different sensor behavior between NO_2 and reducing species such as ethanol and water under light activation might be supported by the mechanism proposed by Nasriddinov et al. [42]. During illumination, electron-hole pairs are formed, resulting in an increase in electron concentration and photodesorption of oxygen from the surface. This results in a decrease in the concentration of chemisorbed oxygen, whose sites can be replaced by water molecules and hydroxyl groups. Moreover, this might have as a consequence, oxidizing gases are adsorbed more efficiently, further increasing resistance, while the response to reducing gases is attenuated due to the reduced availability of chemisorbed oxygen.

With regard to UV-light activation, the ZnO sensing mechanism was already studied by *in-situ* DRIFT measurements for NO_2 detection, highlighting the formation of nitrites and nitrates on the ZnO film surface [43], also confirmed by *AB* spectrum on ZnO powder in the present work (Fig. 5, orange line). On the contrary, for ethanol and water the detection process under UV light has only been hypothesized based on electrical characterization to date [44,45], then the absence of experimental evidence to further explore the surface chemical reactivity may result in speculative conclusions. For instance, Alenezi et al. proposed that the decrease in ZnO resistance during exposure to ethanol could be attributed to the interaction between the analyte and O_2^- present on the surface, going through a supposed intermediate reaction involving acetaldehyde, realizing electrons in the *CB* [44].

In this context, the present study contributes to bridging this gap by providing direct spectroscopic evidence of surface reactions, as follows. The broad band 3600 −2900 cm^{-1} identified in all the three spectra (Figs. 2b, 3b, 4b) corresponds to the formation of hydrogen bonds [46]. This type of intermolecular forces is a common occurrence in the physisorption process, wherein water molecules bind to the oxygen or hydroxyl groups on the metal-oxide surface, as shown in Fig. S20a and S20b. Similarly, hydrogen bonds can be formed between an oxygen of the NO_2 molecule and a surface hydroxyl group (Fig. S20c). In the latter case, the *AB* band peak is shifted to lower wavenumbers. This physisorption creates superficial dipoles over the film, which is consistent with the changes in resistance.

Under blue-light irradiation (Fig. 3b), a broad band of reduced intensity persists for NO_2 and ethanol. In this regard, the lower response and lack of recovery can be attributed to the reduced production of electron-hole pairs under blue-light irradiation. Electron excitation from donor levels generates localized holes within the material that may not contribute to photoinduced gas adsorption or desorption, resulting in a weak and irreversible response [9]. This phenomenon can also hinder the establishment of a dynamic equilibrium, preventing the signal from stabilizing into a plateau during gas injection.

The *AB* spectra acquired under green-light irradiation (Fig. 4b) did not exhibit any peak in presence of NO_2 and ethanol, consistent with the absence of sensor response under these conditions. In contrast, the *AB* spectra at 20 RH% showed the features previously detected under other illumination regimes, indicating the persistence of physisorbed water on the surface. This suggests that the photon energy associated with green-light irradiation, while possibly sufficient to induce a limited generation of charge carriers, is inadequate to activate the adsorption and desorption processes required for gas sensing. As a result, no surface species are formed or removed to impact the material electrical properties in the presence of NO_2 and ethanol. At the same time, physisorbed water molecules may interact with the ZnO film through weak surface interactions that are insufficient to significantly modify its resistance, thereby failing to induce a sensor response. This behavior may also be attributed to the inefficient activation energy provided by green-light irradiation.

In summary, the *AB* spectra collected over the ZnO sensing film primarily indicated the formation of hydrogen bonds resulting from the physisorption of analyte molecules, which can slightly modify the electrical properties of the film by creating superficial dipoles, *i.e.* weak interactions. Nevertheless, this interaction only occasionally correlates with a sensor response, so the sensor behavior remains partially hidden. In addition to physisorption, the ZnO surface can undergo reduction through the action of H_2O and ethanol, or oxidation by NO_2. If the extent of these chemisorption reactions is small enough, the formation of reaction products may not be detectable in the *AB* spectra collected with a small spot, such as the 2.5 mm spot used in the *operando* DRIFT set-up on the working sensor. In contrast, the *in-situ* characterization on the ZnO powder allows the use of larger IR spots (3.5 mm), increasing the number of counts and consequently facilitating the detection of subtle variations in surface chemistry. Moreover, these different experimental conditions have the potential to exert a substantial influence on the signal-to-noise ratio, as highlighted by DRIFT spectra acquired on the ZnO sensing film (Figs. 2b, 3b, 4b) and on the powder (Fig. 5).

Comparing *in-situ* and *operando* characterizations could validate the proposed sensing mechanism or enrich the information achieved by DRIFT spectroscopy. Indeed, the *AB* spectra collected over the UV-LED activated ZnO powder during the injection of the analytes, besides the characteristic band associated with gas physisorption, showed additional peaks corresponding to the formation of chemisorbed species. In particular, NO_2 generates nitrato and bidentate nitrate species, while ethanol generates ethoxy and acetate species, which may serve as intermediates in the dehydrogenation of ethanol to form diethyl ether, acetic acid or other byproducts [47]. Furthermore, the dissociation of H_2O results in the formation of hydroxyl groups. Even in negligible quantities, these reactions have the capacity to modify the surface charge and the concentration of major charge carriers in the material. Concurrently, dipole formation due to physisorption exerts an influence on the overall variation in ZnO film resistance.

The setup configuration is complemented by the ability to perform *in-situ* measurements on the photoactivated powder. Indeed, the present work has demonstrated that the presence of chemical species adsorbed on the surface of the sensing layer does not always correspond to observable peaks in the *AB* spectrum. This is due to the limited probability of such reactions occurring, which complicates their identification on the sensing device (Figs. 2b, 3b, 4b), while the same analyses on the functional powder (Fig. 5) are capable of revealing these chemical species.

5. Conclusions

This work represents a significant step towards addressing the lack of knowledge regarding SMOX chemoresistive gas sensors in photoactivation, enabling a deeper understanding of the gas sensing mechanism and investigating material photosensitivity. An innovative configuration for *operando* DRIFTS characterization at RT was validated, using customized add-on tools, on both gas sensors and their relative functional nanostructured powders in properly calibrated photoactivation mode, at three different wavelengths. ZnO was used as a gold standard and tested in presence of NO_2, ethanol, and humidity. During the electrical characterizations, the ZnO sensor performed as expected and exhibited optimal results under UV-light illumination. Instead, the contextually acquired *AB* spectra provided insights into the gas sensing mechanism. Indeed, the *operando* DRIFT spectra revealed the physisorption of the target gas on the sensing layer through the formation of hydrogen bonds between the analyte molecules (NO_2, CH_3CH_2OH and H_2O) and hydroxyl groups on the surface. However, the observed change in resistance could not be fully explained by physisorption alone, suggesting the potential presence of chemisorbed species on the surface. These species could be undetectable if present at low

concentrations on the sensor surface, necessitating further investigation. In this perspective, the material was subjected to *in-situ* DRIFTS measurements on the functional powder under UV-light irradiation. In addition to the characteristic band associated with gas physisorption, these measurements revealed the presence of additional peaks which were attributed to the formation of chemisorbed species. Indeed, NO_2 generates nitrato and bidentate nitrate species, while ethanol produces ethoxy and acetate species. These chemisorptions induce resistance changes, which could be further investigated by RT chemisorption analysis [48,49]. Nevertheless, additional operando DRIFT analysis using deuterated gases (D_2, D_2O) [50] may provide further insights into the composition and chemistry of water-related surface species and metal-oxide lattice overtones, through comparison of H_2O and D_2O spectra [51].

The development of technologies for low-power consumption - on the order of tens of milliwatts - and the monitoring of hazardous gases in specific contexts, such as medical applications and cultural heritage preservation, is contingent upon a deeper knowledge of RT operating devices. Moreover, this is leading to a viral overspreading of miniaturized devices in which sensing layers and light-emitting elements are embedded, *e.g.*, for portable/wearable sensors, with a power consumption in the order of μW [52,53].

CRediT authorship contribution statement

Emanuela Tavaglione: conceptualization, methodology, formal analysis, investigation, data curation, writing - original draft, visualization. **Elena Spagnoli:** methodology, validation, formal analysis, investigation, data curation, writing - review & editing, visualization. **Matteo Valt:** conceptualization, formal analysis, writing - review & editing. **Paolo Bernardoni:** conceptualization, methodology. **Michele Della Ciana:** conceptualization. **Federico Bottegoni:** conceptualization, methodology, writing - review & editing. **Margherita Negri:** investigation, data curation. **Francesco Scali:** Methodology, Formal Analysis, Investigation, Data Curation, Visualization. **Carlo Zucchetti:** conceptualization, methodology. **Matteo Ferroni:** formal analysis, investigation. **Matteo Ardit:** Formal Analysis, Investigation, Writing - Review & Editing. **Lia Vanzetti:** Formal Analysis, Investigation. **Vito Cristino:** Formal Analysis, Investigation. **Francesco Di Benedetto:** investigation, data curation. **Barbara Fabbri:** conceptualization, methodology, validation, writing - original draft, visualization, supervision, project administration, funding acquisition.

Declaration of Competing Interest

The authors declare that they have no known competing financial interests or personal relationships that could have appeared to influence the work reported in this paper.

Acknowledgments

This work was funded by PRIN 2022 "2022LZKWW3 - Visible light activated gas sensors based on semiconductors: an operando investigation by DRIFT and confocal micro-Raman spectroscopy (LEVANTO)" - funded by the UE - NextGenEU - M4C2, Inv.1.1 - CUP: F53D23001100001.

This publication was produced while attending the doctoral course in Physics (E. Tavaglione) at the University of Ferrara, cycle 39, with the support of a scholarship funded by the D.M. n. 118/2023, supported by PNRR - funded by the UE - NextGenerationEU - Mission 4 "Education and Research" - Component 1 "Strengthening the offer of educational services: from nursery schools to university" - Investment 4.1 PNRR scholarships for Cultural Heritage.

The authors are indebted to Sandra Ristori, for granting the access to the EPR instrumentation at the Dept. of Chemistry of the University of Florence, and to Alfonso Zoleo and Riccardo Punis of the Dept. of Chemical Sciences of the University of Padova, for the help in the calibration of the spectrometer.

Appendix A. Supporting information

Supplementary data associated with this article can be found in the online version at doi:10.1016/j.snb.2025.138504.

Data availability

Data will be made available on request.

References

[1] R. Kumar, X. Liu, J. Zhang, M. Kumar, Room-Temperature gas sensors under photoactivation: from metal oxides to 2D materials, NanoMicro Lett. 12 (1) (2020) 164, https://doi.org/10.1007/s40820-020-00503-4.
[2] S.M. Majhi, A. Mirzaei, H.W. Kim, S.S. Kim, T.W. Kim, Recent advances in energy-saving chemiresistive gas sensors: a review, Nano Energy 79 (2021) 105369, https://doi.org/10.1016/j.nanoen.2020.105369.
[3] F. Xu, H.-P. Ho, Light-Activated metal oxide gas sensors: a review, Micromachines 8 (11) (2017) 333, https://doi.org/10.3390/mi8110333.
[4] S.-W. Fan, A.K. Srivastava, V.P. Dravid, Nanopatterned polycrystalline ZnO for room temperature gas sensing, Sens. Actuators B Chem. 144 (1) (2010) 159–163, https://doi.org/10.1016/j.snb.2009.10.054.
[5] H. Lüth, Solid surfaces, interfaces and thin films. Graduate Texts in Physics. Cham, Springer International Publishing, Berlin, 2015, https://doi.org/10.1007/978-3-319-10756-1.
[6] A. Oprea, D. Degler, N. Barsan, A. Hemeryck, J. Rebholz, Basics of semiconducting metal oxide–based gas sensors. Gas Sensors Based on Conducting Metal Oxides, Elsevier, Amsterdam, 2019, pp. 61–165, https://doi.org/10.1016/B978-0-12-811224-3.00003-2.
[7] S. Ganesh Moorthy, M. Bouvet, Effects of visible light on gas sensors: from inorganic resistors to molecular material-based heterojunctions, Sensors 24 (5) (2024) 1571, https://doi.org/10.3390/s24051571.
[8] S.-W. Fan, A.K. Srivastava, V.P. Dravid, UV-activated room-temperature gas sensing mechanism of polycrystalline ZnO, Appl. Phys. Lett. 95 (14) (2009) 142106, https://doi.org/10.1063/1.3243458.
[9] E. Espid, F. Taghipour, UV-LED Photo-activated chemical gas sensors: a review, Crit. Rev. Solid State Mater. Sci. 42 (5) (2017) 416–432, https://doi.org/10.1080/10408436.2016.1226161.
[10] A. Gaiardo, et al., ZnO and Au/ZnO thin films: room-temperature chemoresistive properties for gas sensing applications, Sens. Actuators B Chem. 237 (2016) 1085–1094, https://doi.org/10.1016/j.snb.2016.07.134.
[11] N.D. Chinh, et al., Adsorption/desorption kinetics of nitric oxide on zinc oxide nano film sensor enhanced by light irradiation and gold-nanoparticles decoration, Sens. Actuators B Chem. 281 (2019) 262–272, https://doi.org/10.1016/j.snb.2018.10.113.
[12] X.-X. Wang, B. Junker, C. Ewald, U. Weimar, X. Guo, N. Barsan, Proof of concept for operando infrared spectroscopy investigation of light-excited metal oxide-based gas sensors, J. Phys. Chem. Lett. 13 (16) (2022) 3631–3635, https://doi.org/10.1021/acs.jpclett.2c00480.
[13] A. Rossi, et al., Functionalization of indium oxide for empowered detection of CO_2 over an extra-wide range of concentrations, ACS Appl. Mater. Interfaces 15 (28) (2023) 33732–33743, https://doi.org/10.1021/acsami.3c04789.
[14] M. Valt, M.D. Ciana, B. Fabbri, D. Sali, A. Gaiardo, V. Guidi, Design and validation of a novel operando spectroscopy reaction chamber for chemoresistive gas sensors, Sens. Actuators B Chem. 341 (2021) 130012, https://doi.org/10.1016/j.snb.2021.130012.
[15] E. Spagnoli, M. Valt, A. Gaiardo, B. Fabbri, V. Guidi, Insights into the sensing mechanism of a metal-oxide solid solution via operando diffuse reflectance infrared

Fourier transform spectroscopy, Nanomaterials 13 (19) (2023) 2708, https://doi.org/10.3390/nano13192708.
[16] C. Zucchetti, et al., Non-local architecture for spin current manipulation in silicon platforms, APL Mater. 11 (2) (2023) 021102, https://doi.org/10.1063/5.0130759.
[17] F. Bottegoni, C. Zucchetti, G. Isella, M. Bollani, M. Finazzi, F. Ciccacci, Spin-charge interconversion in heterostructures based on group-IV semiconductors, Riv. Nuovo Cim. 43 (2) (2020) 45–96, https://doi.org/10.1007/s40766-020-0002-0.
[18] C. Zucchetti, et al., Probing the in-plane electron spin polarization in ge/ si 0.15 ge 0.85 multiple quantum wells, Phys. Rev. B 101 (11) (2020) 115408, https://doi.org/10.1103/PhysRevB.101.115408.
[19] M.D. Ciana, et al., SO_2 sensing mechanism of nanostructured SiC-SiO_xC core shell: an operando DRIFT investigation, Sens. Actuators B Chem. 371 (2022) 132497, https://doi.org/10.1016/j.snb.2022.132497.
[20] E. Spagnoli, et al., Design of a metal-oxide solid solution for selective detection of ethanol with marginal influence by humidity, Sens. Actuators B Chem. 370 (2022) 132426, https://doi.org/10.1016/j.snb.2022.132426.
[21] S. Vettori, E. Cantisani, T. Ismaelli, G. Scardozzi, A. Buccianti, F. Di Benedetto, An EPR study of the marbles from quarries of the denizli region (Turkey): a contribution to the provenance assessment of materials with close relationships, Microchem. J. 202 (2024) 110802, https://doi.org/10.1016/j.microc.2024.110802.
[22] E. Cerrato, M.C. Paganini, E. Giamello, Photoactivity under visible light of defective ZnO investigated by EPR spectroscopy and photoluminescence, J. Photochem. Photobiol. A Chem. 397 (2020) 112531, https://doi.org/10.1016/j.jphotochem.2020.112531.
[23] I. Panžić, A. Bafti, F. Radovanović-Perić, D. Gašparić, Z. Shi, A. Borenstein, V. Mandić, Advancements in nanostructured functional constituent materials for gas sensing applications: a comprehensive review, Appl. Sci. 15 (2025) 2522, https://doi.org/10.3390/app15052522.
[24] S.-L. Gao, L.-P. Qiu, J. Zhang, W.-P. Han, S. Ramakrishna, Y.-Z. Long, Persistent photoconductivity of metal oxide semiconductors, ACS Appl. Electron. Mater. 6 (3) (2024) 1542–1561, https://doi.org/10.1021/acsaelm.3c01549.
[25] V. Bhatt, M. Kumar, J. Kim, H.-J. Chung, J.-H. Yun, Persistent photoconductivity in Al-doped ZnO photoconductors under air, nitrogen and oxygen ambiance: role of oxygen vacancies induced DX centers, Ceram. Int. 45 (7) (2019) 8561–8570, https://doi.org/10.1016/j.ceramint.2019.01.174.
[26] N. Apostolescu, T. Schröder, S. Kureti, Study on the mechanism of the reaction of NO_2 with aluminium oxide, Appl. Catal. B Environ. 51 (1) (2004) 43–50, https://doi.org/10.1016/j.apcatb.2004.02.003.
[27] H. Noei, H. Qiu, Y. Wang, E. Löffler, C. Wöll, M. Muhler, The identification of hydroxyl groups on ZnO nanoparticles by infrared spectroscopy, Phys. Chem. Chem. Phys. 10 (47) (2008) 7092, https://doi.org/10.1039/b811029h.
[28] B. Zhang, J.-Y. Sun, P.-X. Gao, "Low-Concentration NOx gas analysis using single bimodular ZnO nanorod Sensor,", ACS Sens. 6 (8) (2021) 2979–2987, https://doi.org/10.1021/acssensors.1c00834.
[29] K.I. Hadjiivanov, Identification of neutral and charged nx oy surface species by IR spectroscopy, Catal. Rev. 42 (1–2) (2000) 71–144, https://doi.org/10.1081/CR-100100260.
[30] C. Ewald, N. Saito, U. Weimar, N. Barsan, Role of potassium loading in ZnO-based gas sensors under NO_2 exposure – operando diffuse reflectance infrared Fourier transform spectroscopic study, Sens. Actuators B Chem. 393 (2023) 134321, https://doi.org/10.1016/j.snb.2023.134321.
[31] J. Llorca, N. Homs, P. Ramirez De La Piscina, In situ DRIFT-mass spectrometry study of the ethanol steam-reforming reaction over carbonyl-derived Co/ZnO catalysts,", J. Catal. 227 (2) (2004) 556–560, https://doi.org/10.1016/j.jcat.2004.08.024.
[32] J. Gao, A.V. Teplyakov, Surface species formed during thermal transformation of ethanol on ZnO powder, J. Catal. 300 (2013) 163–173, https://doi.org/10.1016/j.jcat.2012.12.026.
[33] T. Shinkai, J.K.C.N. Agutaya, B. Manna, M. Boepple, M. Iwai, K. Masumoto, K. Koga, K. Kawanami, Y. Nakamura, A.T. Quitain, K. Suematsu, Y. Inomata, N. Barsan, T. Kida, Ethanol sensing mechanism of ZnO nanorods revealed by DRIFT spectroscopy and DFT calculations, J. Mater. Chem. A 12 (2024) 7564–7576, https://doi.org/10.1039/d3ta06486g.
[34] F. Viñes, A. Iglesias-Juez, F. Illas, M. Fernández-García, Hydroxyl identification on ZnO by infrared spectroscopies: theory and experiments, J. Phys. Chem. C. 118 (3) (2014) 1492–1505, https://doi.org/10.1021/jp407021v.
[35] S. Lany, A. Zunger, Anion vacancies as a source of persistent photoconductivity in II-VI and chalcopyrite semiconductors, Phys. Rev. B 72 (3) (2005) 035215, https://doi.org/10.1103/PhysRevB.72.035215.
[36] R.G. Ulbrich, "Low density photoexcitation phenomena in semiconductors: aspects of theory and experiment,", SolidState Electron. 21 (1) (1978) 51–59, https://doi.org/10.1016/0038-1101(78)90114-4.
[37] A. Janotti, C.G. Van De Walle, Native point defects in ZnO, Phys. Rev. B 76 (16) (2007) 165202, https://doi.org/10.1103/PhysRevB.76.165202.
[38] C. Zucchetti, et al., Hole and electron spin lifetime in lightly n -doped silicon at low temperatures, Appl. Phys. Lett. 125 (17) (2024) 172404, https://doi.org/10.1063/5.0223099.
[39] B. Fabbri, et al., Electrical, optical and sensing properties of photo-activated ZnO thin films, Procedia Eng. 87 (2014) 148–151, https://doi.org/10.1016/j.proeng.2014.11.605.
[40] J. Gong, Y. Li, X. Chai, Z. Hu, Y. Deng, UV-light-activated ZnO fibers for organic gas sensing at room temperature, J. Phys. Chem. C. 114 (2) (2010) 1293–1298, https://doi.org/10.1021/jp906043.
[41] B. Fabbri, et al., Chemoresistive properties of photo-activated thin and thick ZnO films, Sens. Actuators B Chem. 222 (2016) 1251–1256, https://doi.org/10.1016/j.snb.2015.06.048.
[42] A. Nasriddinov, R. Zairov, M. Rumyantseva, Light-activated semiconductor gas sensors: pathways to improve sensitivity and reduce energy consumption, Front. Chem. 13 (2025), https://doi.org/10.3389/fchem.2025.1538217.
[43] J. Wang, Y. Shen, X. Li, Y. Xia, C. Yang, Synergistic effects of UV activation and surface oxygen vacancies on the room-temperature NO_2 gas sensing performance of ZnO nanowires, Sens. Actuators B Chem. 298 (2019) 126858, https://doi.org/10.1016/j.snb.2019.126858.
[44] M.R. Alenezi, A.S. Alshammari, K.D.G.I. Jayawardena, M.J. Beliatis, S.J. Henley, S. R.P. Silva, Role of the exposed polar facets in the performance of thermally and UV activated ZnO nanostructured gas sensors, J. Phys. Chem. C. 117 (34) (2013) 17850–17858, https://doi.org/10.1021/jp4061895.
[45] C.-L. Hsu, L.-F. Chang, T.-J. Hsueh, Light-activated humidity and gas sensing by ZnO nanowires grown on LED at room temperature, Sens. Actuators B Chem. 249 (2017) 265–277, https://doi.org/10.1016/j.snb.2017.04.083.
[46] M. Takeuchi, L. Bertinetti, G. Martra, S. Coluccia, M. Anpo, States of H_2O adsorbed on oxides: an investigation by near and mid infrared spectroscopy, Appl. Catal. Gen. 307 (1) (2006) 13–20, https://doi.org/10.1016/j.apcata.2006.03.002.
[47] A.P. Soares Dias, B. Rijo, M.F. Costa Pereira, R. Zăvoianu, O.D. Pavel, Valorization of (Bio)ethanol over MoO_3/(WO_3-ZrO_2) sol-gel-like catalysts, Reactions 5 (1) (2024) 260–273, https://doi.org/10.3390/reactions5010012.
[48] A. Marikutsa, A. Novikova, M. Rumyantseva, N. Khmelevsky, A. Gaskov, Comparison of Au-functionalized semiconductor metal oxides in sensitivity to VOC, Sens. Actuators B Chem. 326 (2021) 128980, https://doi.org/10.1016/j.snb.2020.128980.
[49] I.C. Weber, P. Rüedi, P. Šot, A.T. Güntner, S.E. Pratsinis, Handheld device for selective benzene sensing over toluene and xylene, Adv. Sci. 9 (2022) 2103853, https://doi.org/10.1002/advs.202103853.
[50] R.G. Pavelko, J.-K. Choi, A. Urakawa, M. Yuasa, T. Kida, K. Shimanoe, H_2O/D_2O exchange on SnO_2 materials in the presence of CO: operando spectroscopic and electric resistance measurements, J. Phys. Chem. C. 118 (2014) 2554–2563, https://doi.org/10.1021/jp4108766.
[51] D. Degler, B. Junker, F. Allmendinger, U. Weimar, N. Barsan, Investigations on the Temperature-Dependent interaction of water vapor with tin dioxide and its implications on gas sensing, ACS Sens. 5 (2020) 3207–3216, https://doi.org/10.1021/acssensors.0c01493.
[52] K. Lee, I. Cho, M. Kang, J. Jeong, M. Choi, K.Y. Woo, K.-J. Yoon, Y.-H. Cho, I. Park, Ultra-Low-Power E-Nose system based on Multi-Micro-LED-Integrated, nanostructured gas sensors and deep learning, ACS Nano 17 (2022) 539–551, https://doi.org/10.1021/acsnano.2c09314.
[53] I. Cho, K. Lee, Y.C. Sim, J.-S. Jeong, M. Cho, H. Jung, M. Kang, Y.-H. Cho, S.C. Ha, K.-J. Yoon, I. Park, Deep-learning-based gas identification by time-variant illumination of a single micro-LED-embedded gas sensor, Light Sci. Appl. 12 (2023), https://doi.org/10.1038/s41377-023-01120-7.

E. Tavaglione obtained her M.Sc. degree in Physics (Magna cum Laude) at the University of Ferrara, in 2023. Currently, she is a Ph.D. student in Physics at the University of Ferrara, working in the field of chemoresistive gas sensors on photo-activation, *operando* DRIFT spectroscopy and data analysis through machine learning algorithms.

E. Spagnoli obtained her M.Sc. degree in Chemistry (Magna cum Laude) at the University of Ferrara in 2019. She received her Ph.D. in Physics at the University of Ferrara in 2023. Currently, she is a PostDoc at the University of Ferrara. Her current research interests are related to *operando* DRIFT spectroscopy applied to chemoresistive gas sensors, and the synthesis and characterization of nanostructured semiconductors for the development of functional sensing films.

M. Valt obtained his Ph.D. degree in Physics in March 2020 with a thesis titled: "2D materials for room-temperature chemiresistive gas sensing" at the University of Ferrara. Previously, he obtained his M.Sc. degree in Chemistry with a thesis on Functionalization of Graphene Oxide for Gas Sensing and Cation Trapping. He is a researcher in the Sensors and Devices center of the Bruno Kessler Foundation. His current research interests are related to the development and employment of novel materials for chemiresistive gas sensing in diverse fields of applications.

P. Bernardoni holds an M.Sc. in Physics from the University of Ferrara (2012) and a Ph.D. in Physics from the same institution (2016). His research has focused on semiconductor physics, optics, and electronics. Currently, he is working as an R&D Engineer at G&W Altea S.r.l., where he is involved in the development of advanced voltage sensors.

M. Della Ciana obtained his M.Sc. degree in physics of matter at the University of Bologna in 2018 and his Ph.D. degree in Physics in 2022 at University of Ferrara in collaboration with the Institute for microelectronics and microsystems (CNR) of Bologna. Currently, he is working at Sacmi Imola S.C.

F. Bottegoni obtained his Ph.D. in Physics with honors in 2012 at Politecnico di Milano. He is currently associate professor at the Physics Department of Politecnico di Milano and scientific director of the SemiSpin laboratory at Politecnico di Milano. He deals with spin generation, transport and manipulation in semiconductor platforms and semiconductor heterostructures, topological insulators and low dimensional materials.

M. Negri obtained her M.Sc. degree in Physics Engineering at Politecnico di Milano, in 2024. Her thesis work has been about the modulation of spin currents by means of the spin Hall effect in bulk germanium.

F. Scali graduated in Physics Engineering at the Politecnico di Milano, Italy in 2022 and is currently enrolled as Ph.D. student at Physics Department of the same institution. The topic of F. S. 's Ph.D. research is the study of spin transport in semiconductors, which involves the manipulation of spin currents in solid-state systems with electric fields, strain and spin-orbit coupling. He is currently exploiting confocal microscopy techniques for optical injection of spin-polarized carriers and investigating spin-to-charge conversion phenomena for spin detection.

C. Zucchetti received his PhD in Physics with honors in 2019 defending a dissertation on spin transport and spin-charge interconversion in Ge-based structures. He is currently assistant professor at the Department of Physics at Politecnico di Milano, in Milan. His research focuses on semiconductor-based spintronics, mainly explored by optically injecting spin-polarized carriers in the semiconductors. He worked on spin-charge interconversion phenomena like spin-Hall effect and Rashba-Edelestein effect, and uniaxial magnetoresistance in Ge.

M. Ferroni received the PhD degree in Physics at the University of Ferrara in 1998, and presently is associate professor in Experimental Physics at the University of Brescia. He collaborates with the Bologna Section of the Institute for Nanostructured Materials (ISMN) of the National Research Council (CNR). His research activity concerns the characterization of nanostructured materials by means of transmission and scanning electron microscopy.

M. Ardit received his Ph.D. in Mineralogy and Crystallography from the University of Ferrara in 2012. He is currently Associate Professor at the Department of Earth Sciences at the University of Padova. His research activity is mainly aimed at understanding the structural properties of minerals and synthetic analogs, to provide the basis for the design of materials with enhanced properties and to understand structural dynamics under different chemical and physical conditions.

L. Vanzetti attended the University of Parma, where she received the degree in Physics and a Master's degree in Materials Science and Technology in 1985 and 1988, respectively. She is currently a senior researcher at SD-MNF facility of the Fondazione Bruno Kessler, Trento (Italy) and in charge of the XPS instrument. Her research interests cover different fields, spanning from microelectronics to biomaterials and bio-interfaces, to sensors.

V. Cristino obtained his PhD. in Chemistry at University of Ferrara in 2011. Currently he is a Researcher at the Department of Environmental Sciences and Prevention of the University of Ferrara, working in the field of nanostructured metal-oxide photoanodes for solar energy conversion and environmental remediation.

B. Fabbri obtained her Ph.D. in Physics at University of Ferrara in 2015. Currently she is a Researcher involved in the field of gas sensors at Sensors Lab of Ferrara University. She studies all key aspects involved in the study and development of solid-state gas sensors. In particular, she is interested in innovative and sustainable nanostructured materials, gas sensor applications and their characterization through *operando* approaches.